Short-time Dynamics of Frictional Strength in Dry Friction

O. Ben-David, G. Cohen and J. Fineberg

The Racah Institute of Physics, The Hebrew University of Jerusalem, Givat Ram, Jerusalem 91904, Israel.

We present an experimental study of the onset of local frictional motion along a long, spatially extended interface that separates two PMMA blocks in dry frictional contact. At applied shear forces significantly below the static friction threshold, rapid precursory detachment fronts are excited, which propagate at near sound speeds along the interface. These fronts initiate from the interface edge and arrest prior to traversing the entire sample length. Along the fronts' path, we perform real-time measurements of the real contact area at every spatial point within the interface. In addition, the motion (slip) of the material adjacent to the interface is simultaneously measured at chosen locations. Upon their arrival at each spatial point along their path, these fronts instantaneously (within 4μsec) reduce the net contact area. Net slip is only initiated *after* this contact area reduction occurs. Slip is initially rapid and progresses at its initial velocity for a constant (60μsec) duration. Slip dynamics then undergo a sharp transition to velocities an order of magnitude slower, which remain nearly constant until slip arrest. We demonstrate that this scenario can be quantitatively explained by a model of interface weakening caused by instantaneous fracture-induced heating. Sustained rapid slip occurs in this weakened phase. Once the interface cools beneath its glass temperature the sharp transition to slow slip takes place. A similar fracture-induced weakening scenario might be expected in additional classes of materials.

Key words: Contact Mechanics, Friction Mechanisms, Static Friction, Stick-Slip, Unlubricated Friction, Polymers (solid), fracture induced weakening

1. Introduction

The short-time dynamics of dry friction are of fundamental interest in fields ranging from hard drive disk [1] design to the study of earthquakes [2-5]. The evolution of frictional strength at the interface of separation between two elastic bodies can have a profound influence on both very slow and very rapid sliding processes. Here, we restrict our attention to frictional interfaces in which there is no intervening lubrication layer. These interfaces are generically rough, where the relevant roughness scale may vary from sub-micron scales in storage devices, to meters where frictional motion between tectonic

plates is considered. Due to their rough nature, dry frictional interfaces are composed of a large ensemble of discrete micro-contacts. The *real* contact area is generally, at most, a few percent of the nominal cross-section of the contact interface. Frictional strength is given by [6] $A\tau$, where A is the amount of real contact area and τ the shear strength of the individual contacts. Both $A(x,t)$ and $\tau(x,t)$ may vary spatially, and evolve with time or with slip, so that each is a dynamic variable (where t and $\boldsymbol{x}$ denote time and position respectively).

In order to induce motion at a frictional interface, the frictional strength at each spatial point must be overcome. Recent studies [7-10] have shown that the transition from static to dynamic friction (i.e. from stick to slip) is mediated by collective motion along the interface that is embodied by rapid crack-like detachment fronts. These fronts fracture the contacts at the interface and facilitate movement. Studies have shown [10] that when the externally applied shearing force, F_s, is not uniformly distributed, a sequence of precursory arrested cracks may propagate through part of the interface. The passage of these precursory fronts both reduces A and enables local frictional motion (slip) at all points along their path. Slip, $\delta(X,t)$, will evolve at any given location, X, traversed by a detachment front (either arrested or not). No slip will occur prior to a front's arrival.

The dynamic evolution of the frictional strength is closely linked to the rapid processes of contact detachment and subsequent reattachment that are precipitated by these fronts. This evolution must, of course, enable the mean (slow) motion of frictionally sliding bodies. Although empirical friction laws provide an excellent phenomenological description of this slow evolution, it is currently unclear how this description evolves from the rapid dynamics described above. The experiments described below provide an initial step in this direction. To this end, we will describe the evolution of $\delta(X,t)$ and $A(X,t)$ before, during, and after the passage of a detachment front, in conjunction with measurement of $A(x,\underline{t})$ along the entire frictional interface.

2. Experimental system

The majority of our experiments were conducted using long and thin acrylic blocks of PMMA (Poly-methyl-methacrylate) with spatial dimensions of 200mm×6mm×100mm (top block) and 300mm×30mm×28mm (base block), in the sliding (x), transverse (y) and loading (z) directions. The optically flat sliding surfaces of the top and base blocks were roughened to approximately 1μm r.m.s. Sound velocities in our samples were measured using time-of-flight measurements of ultrasonic pulses, yielding longitudinal and shear wave velocities of c_L=2730m/s and c_S=1370m/s, respectively. The Rayleigh wave, c_R speed in this material is accordingly [11] 1280m/s.

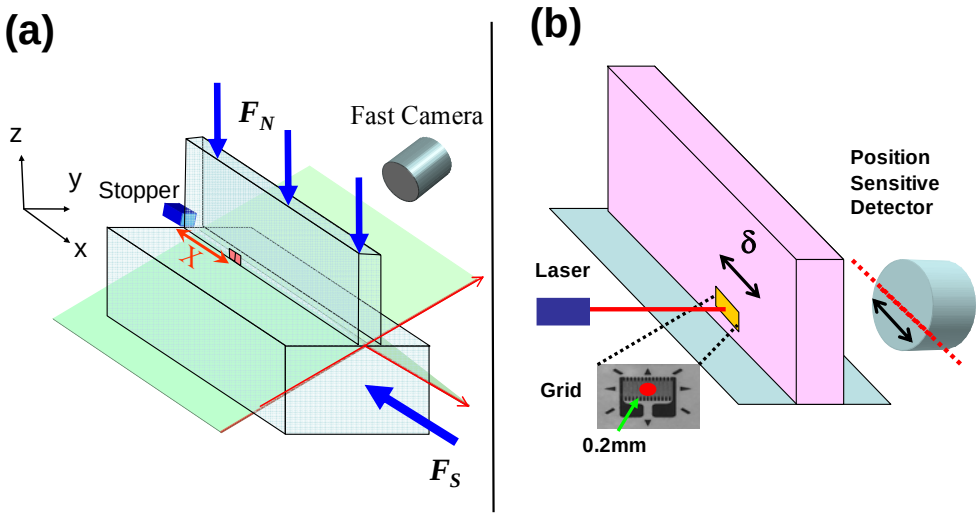

Figure 1. Schematic view of the experimental setup. A uniform normal load, F_N, was applied to two PMMA blocks (Top block and Bottom block). Shear loading F_S was applied to the bottom block which was mounted on a low friction stage constrained to move along the x direction. A rigid stopper adjacent to the trailing edge (x=0) of the Top block restricted its movement in the x direction. Slip was measured simultaneously at both the Top block's leading edge (at x=200mm) and chosen locations X along the interface. The contact area $A(x,t)$ along the entire frictional interface was imaged as in [12] at 4μsec intervals. **b** Slip measurements, $\delta(t)$, were performed at a chosen location, X. A laser beam was focused on a metallic grid glued to the side of the top block approximately 2mm above the frictional interface. The resulting diffraction pattern was focused onto a Position Sensitive Detector (PSD) located 60-70cm from the grid. Displacement of the grid along the x direction caused a corresponding motion of the diffraction pattern, whose "center-of-mass" was proportional to the PSD output voltage. This yielded the displacement $\delta(t)$ at measurement rates of up to 1MHz to 0.2μm resolution.

A schematic description of the experimental system is presented in Figure 1. The two PMMA blocks were pressed together with a uniform load F_N. F_N was monitored throughout the experiment via an S-Beam load cell with a stiffness of 10^7N/m. Shear force, F_S, was applied to the system as follows. The

Bottom block was mounted on a low friction linear stage, its motion in the x direction constrained only by the frictional force at the interface with the Top block. At the trailing edge, x=0, of the Top block a rigid stopper pressing its y-z edge constricted its motion in the x direction. F_S was applied to the Bottom block via an additional load cell (whose stiffness was 10^6N/m) in the negative x direction. An acoustic sensor mounted on the trailing edge of the sample was used to detect slip events. Upon detection of a slip event, the otherwise linear increase in F_S was held for a pre-defined hold time. The hold time was varied from 5-100sec in the experiments described here.

Slip was initiated at the trailing edge, x=0 mm, in the positive x direction. The method of measuring slip, $\delta(X,t)$, at a single point, X, is schematically described in Figure 1b. A 670nm diode laser beam was focused to a spot size of ~0.2mm and passed through a miniature metallic grid glued to a face of the slider. The grid was positioned approximately 2mm above the interface. The grid lines, spaced 0.07mm apart formed a diffraction pattern. This pattern was imaged onto a position sensitive detector (PSD) that was situated 60-70cm from the interface. Any motion of the grid shifted the diffraction pattern accordingly. The output voltage of the PSD changes linearly with the displacement of the "center of mass" of the diffraction pattern. This signal, which was calibrated with a Philtech 170 fiber optic displacement sensor, thereby provided a precise measurement of the material displacement at X at μsec temporal resolution.

Throughout the experiments a Philtec D20 fiber optic displacement sensor measured the displacement of the leading edge of the top block at x=200mm. When precursor events were excited, the leading edge of the Top block did not move relative to the Bottom block. Subtraction of the overall movement of the leading edge from the displacement at X measured by the PSD provided the net slip, $\delta(X,t)$. Subtraction of the leading edge displacement was needed to remove global vibrations of the entire system that were induced by any mechanical resonances of the system that were excited by each slip event. This process yielded clean and precise measurements $\delta(X,t)$ with an accuracy of

approximately 0.2μm at measurement frequencies of up to 1MHz. The location X was varied between experiments over the range X=10-70mm.

Measurement of the real contact area, $A(x,t)$ along the interface is described, schematically, in Figure 1a. A more detailed description of this measurement technique was provided in [9, 12]. A sheet of laser light is incident on the frictional interface at an angle well beyond the angle of total internal reflection from the acrylic-air interface. When the slider block is pressed onto the base block, contact is made at numerous discrete micro-contacts. In this configuration, incident light is reflected away from the interface at every point where contact does *not* occur. Light is only transmitted across the interface at points of contact. As a result, the light intensity transmitted across the interface at each point is proportional to the amount of real contact area, A, at that location. The transmitted light was imaged by a fast (VDS CMC-1300/485N) camera, which is capable of capturing single line pictures of size 1280pixels at a temporal resolution of 4μsec. Each pixel in the acquired images corresponded to an (x-y) area of 0.2mm×0.8mm. As the mean separation between micro-contact points ranged from 2 to 10μm, each pixel imaged the total contact area of thousands of individual contact points. Spatial smoothing of 10 pixels in the x direction was usually employed to reduce measurement noise. As a result, each pixel was proportional to $A(X,t)$ with a spatial resolution of about 1mm in x and a temporal resolution of 4μs. It is important to note that, due to the long and narrow aspect ratio of our top block, the dynamics along the interface were essentially one-dimensional [9]. Thus, measuring the slip and local contact area as function of x and t, is well justified.

For sufficiently high applied loads, the surfaces can come sufficiently close to allow evanescent waves to play a non negligible role in the transmission of light through the interface. This effect will introduce a nonlinear dependence of the transmitted light intensity as a function of A. We compensated for evanescent contributions by performing the following calibration scheme before each experiment. In parallel with measurements of $A(X)$, the local normal stress at location X was measured by means of a miniature strain gage (Vishay 031 MF). In a typical experiment, F_N was increases from 0 to 6000N. As

the real contact area is proportional to the local normal load [6, 13, 14], a calibration curve of local normal load versus transmitted light intensity was used to correct for any evanescent effects. A similar scheme was used for the global measurements of A in [15]. These methods provide measurements of relative changes of A but do not yield an absolute relation between transmitted intensity and real contact area.

The rapid acquisition of $A(x,t)$ and $\delta(X,t)$ was triggered by a fast acoustic sensor. In parallel, we performed a slow acquisition of both quantities at a measurement rate of 25 Hz. These measurements yielded a continuous record of long-time changes over the duration of the entire experiment. In conjunction with the short timescale, rapid measurements (4μsec temporal resolution) of each slip event, we were, therefore, able to follow the dynamics of the frictional interface over seven orders of magnitude in time.

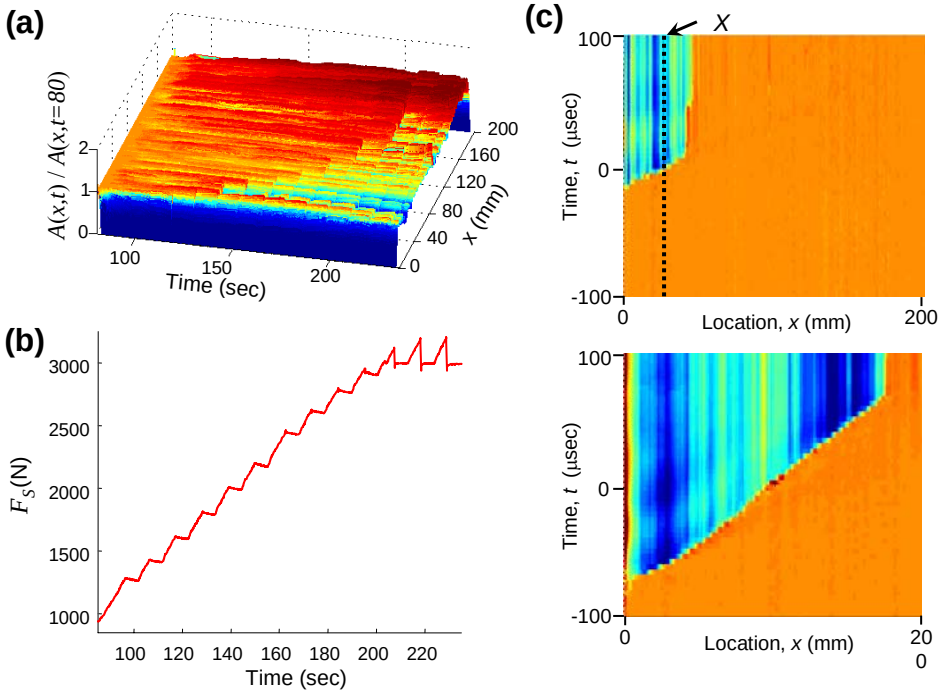

Figure 2. A spatially non-uniform application of F_S triggers a progression of arrested detachment events at shear loads well below the static friction threshold. **a** Measurements of $A(x,t)$, normalized by the value of $A(x,t=80sec)$, throughout an entire experiment. t=0 is the time when F_S was first applied. Hotter colors (reds) indicate increased A while colder colors (blues) indicate reduction of A. Precursors are seen as sharp changes in $A(x,t)$ along part of the interface. Each successive precursor initiates at x=0 and propagates farther along x before arresting. **b** The corresponding loading curve of $F_S(t)$. Upon detection of each precursor event, the increase in F_S was paused for a period of 5-100sec. Slip at x=0, initiated by the precursors, causes small drops in F_S, which are detectable due to the loading system's compliance. Here F_N was 6000N and μ_S = 0.51. **c** Short-time measurements of two precursor events having different propagation lengths. Measurements of $A(x,t)$ at 4μsec intervals reveal that precursors are rapid detachment fronts propagating along the frictional interface at velocities approaching the Rayleigh wave speed of PMMA (c_R = 1280m/s). The precursor velocities are 1200±100m/s **(top panel)** and 1160±40m/s **(bottom panel)**. Here t=0 designates when the front passed the location, X (dotted line in top panel), where $\delta(t)$ was measured. $A(x,t)$ was normalized by it's value 1msec before the front's passage.

3. Results

A series of experiments performed by Rubinstein et al. [10, 16] demonstrated that, when shear forcing is non-uniformly applied a sample's edge, arrested (precursory) slip events occur at shear loads well below the threshold for overall slip of the entire block. These precursor events were shown to be rapid crack-like detachment fronts, which propagate at front velocities approaching the shear wave speed, c_s. Although different in a number of ways from that used by Rubinstein et al. [10], our application of F_S is also spatially non-uniform. We find that, as surmised in [16], this is sufficient to generate qualitatively similar types of precursory events. Figure 2a depicts the contact area along the entire interface while F_S is slowly increased from zero to the static friction threshold. During this increase of F_S a series of progressively growing precursor events takes place. These are seen as abrupt changes in the contact area. Every such event initiated at x=0mm and propagated in the positive x direction. Each subsequent event traversed an increasingly longer distance along the interface before arresting. This progression of discrete precursors continues until a detachment front sweeps through the entire interface and generates a macroscopic stick-slip event. Note that the sequence of precursors transforms the initially uniform profile of $A(x)$ to a highly non-uniform one. As shown in [10], large changes in $A(x)$ are generated by each precursor. The highly non-uniform $A(x)$ profile, formed in this way, is retained even after multiple stick-slip events.

In Figure 2b we present the loading curve, $F_S(t)$, for the (typical) experiment that corresponds to Figure 2a. Small drops in F_S associated with the precursor events can be seen. The sizes of the drops in F_S are proportional to the magnitude of the trailing edge slip induced by each precursor (with the constant of proportionality equal to the load cell stiffness). The step-like form of the loading curve results from the waiting period imposed upon the detection of each precursor (5sec in this example).

Figure 2c presents measurements of two precursor events at 4μsec intervals. The precursors are clearly rapid, attaining front velocities of ~1200m/s (~$0.9c_R$). Each event transpires for less than 100μsec. The contact area is reduced at every location traversed by the precursor. The converse is also

true, *A(x)* does not substantially change beyond the precursor's point of arrest. It is worth noting that arrested precursory events in laboratory experiments are a true analog to earthquakes, since a typical earthquake will only traverse a small portion of a fault before its arrest.

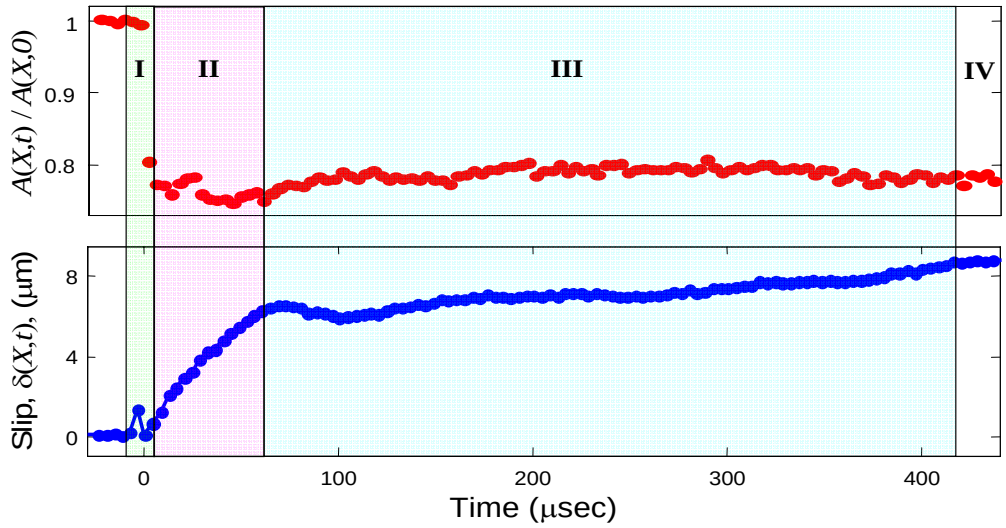

Figure 3. Detachment and evolution of frictional slip during the 500μsec which bracket front passage. Simultaneous measurements of $A(X,t)$ **(top panel)** and $\delta(X,t)$ **(bottom panel)** before, during, and after front passage through location X. The measurements reveal four phases of the dynamics. A detachment phase (Phase I) at t=0 (defined by the front passage time) is followed by rapid slip (Phase II) which sharply transitions into slow slip (Phase III). Note that while A is reduced by ~20% during the detachment phase, it remains relatively constant during the ensuing slip phases. Once slip arrests (t≈400μsec), contact renewal (Phase IV) commences [17].

Each such rapid event provides a well-defined initiation point from which to study the evolution of both A and δ at each location along the front. Let us now consider the detailed dynamics of both $A(X,t)$ and $\delta(X,t)$ before, throughout and after the passage of each precursor event at a selected location, X. Figure 3 depicts the contact area and slip history changes that were caused by a single precursor event at X, as function of time. The figure shows how these evolve over the 500μsec that bracket the front's passage through X. Four distinct phases of the dynamics are seen [17]; detachment (Phase I), rapid slip (Phase II), slow slip (Phase III) and eventual rehealing after slip arrest (Phase IV). We will focus on the short-time dynamics, as described in Phases I-III. The details of the final, rehealing (aging) phase, and the way in which the long-time logarithmic growth of A is normalized for short times, are described elsewhere [17].

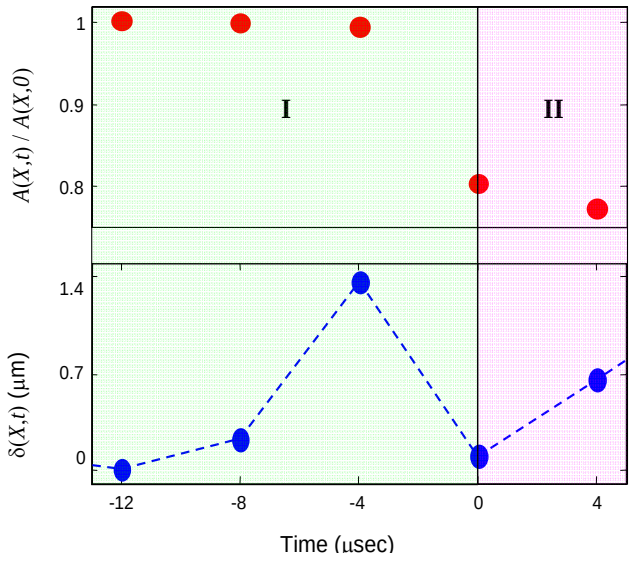

Figure 4. The detachment phase. Typical simultaneous measurements of $A(X,t)$ and $\delta(X,t)$ during Phase I. Nearly all of the reduction of $A(X,t)$ **(top panel)** takes place within our 4μsec temporal resolution. Contact reduction is preceded by a short fluctuation of $\delta(X,t)$ **(bottom panel)** which does not result in net slip.

Figure 4 focuses on the detachment phase. As may be seen in Figure 4 (top), a drop of ~20% in A occurs "immediately", i.e. within our 4μsec temporal resolution. Furthermore, as may be seen in Figure 4 (bottom), no net slip precedes the rapid drop in A. The detachment phase is immediately ***followed*** by net slip. This result is surprising, in the sense that one might naively assume that a reduction in the contact area resulting from shear should occur as a ***result*** of net motion along the interface. In this view, we would expect that the sharp drop in A be accompanied by slip. Figure 4 demonstrates that this is not the case. The rapid fluctuation of δ evident in Figure 4b, immediately precedes the drop in A in all of our experiments. We believe that this fluctuation, which produces no net slip, is related to the structure of the leading edge of the detachment front. We surmise that during this rapid fluctuation, whose magnitude is about the mean extent of a single contact in our system, the surface contacts are actually "broken".

In Figure 5a we present four individual slip events in which the total slip varied by over an order of magnitude. In addition, we present (Figure 5b) a superposition of 16 different slip profiles as a function of time, where the slip is normalized by the total slip in each event. Several characteristic features of all of these different slip profiles are immediately apparent. First, two distinct phases of slip exist; an initial,

very rapid slip phase is followed by a sharp transition to a "slow" slip phase in which slip velocities are an order of magnitude smaller. The initial slip phase is characterized by a high, roughly constant velocity V_{Rapid}, with no apparent acceleration period. During this rapid slip phase, small fluctuations of the contact area are evident. After the sharp transition to the slow slip phase, slip again takes place at an approximately constant velocity, V_{Slow}, before finally arresting. The contact area during the slow phase remains approximately constant throughout its duration. Both phases occur in all events measured.

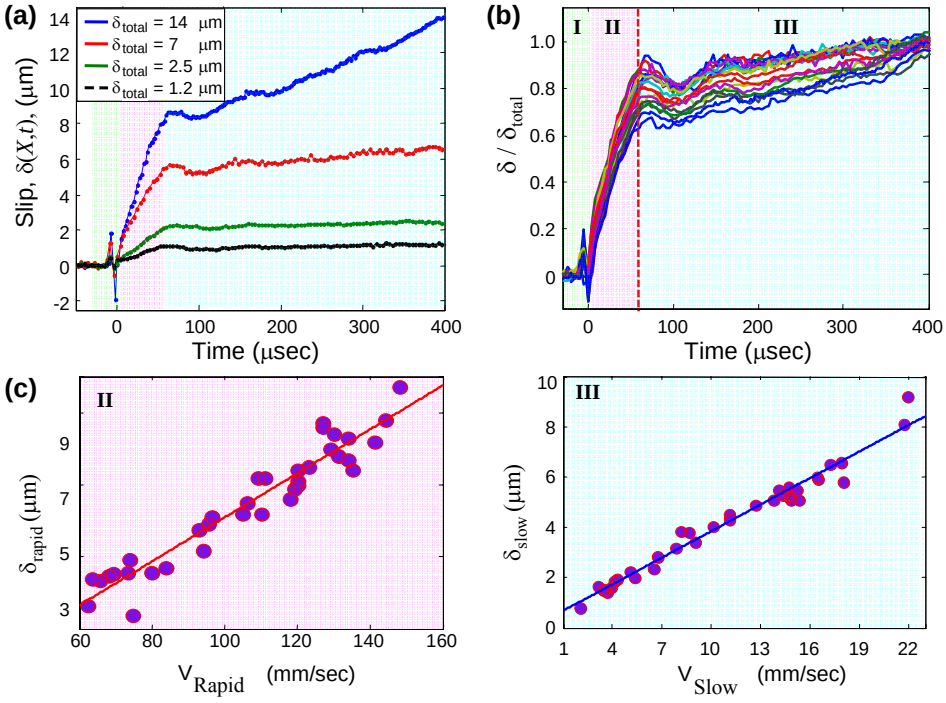

Figure 5. The two phases of frictional slip. **a** Superposition of four typical slip profiles with total slips, δ_{total}, ranging from 1-14μm. All profiles exhibit slip at a roughly constant rapid velocity V_{Rapid} (Phase II) which transitions into slip at constant velocity V_{Slow} (Phase III) which is an order of magnitude slower. **b** Normalizing $\delta(X,t)$ by δ_{total} reveals an approximate collapse of 16 superimposed slip profiles. The collapse indicates that the slip durations, as well as the relative amount of the slip within the two slip phases are approximately constant. The transition from rapid to slow slip is denoted by a dashed line. δ_{total} for the events plotted ranges from 4-20μm. **c** Characteristic timescales of the slip phases. The constant slope of the slip during the rapid slip phase, δ_{Rapid}, as function of V_{Rapid} **(left panel)** reveals the remarkably constant 60μsec duration of the rapid slip phase. Note that this duration is independent of both the amount of slip and slip velocity. A similar plot of δ_{Slow} as function of V_{Slow} **(right panel)** yields a typical 350μsec duration for the slow slip. The solid lines depict linear fits to the data.

The total slip of the events presented in Figure 5b ranges from 4-20μm, with approximately two thirds of the total slip occurring during the rapid slip phase and the remainder within the slow slip phase. It is intriguing that the transition from fast to slow slip velocities occurs at a distinct time scale. As shown in Figures 5b and 5c, the transition from rapid to slow slip always occurs 60±6μsec after slip

initiation. Another time-scale, evident from Figure 5c (right), is the typical duration of the slow slip phase, which was found to be 350±20μsec. The rough collapse of the slip curves in Figure 5b indicates the robust nature of both the overall slip profile and these characteristic time scales. Both time scales were found to be independent of geometrical properties of the system by doubling the width and height of the Bottom block and varying X from 10-70mm with no noticeable effect on the transition time. This transition is also wholly independent of the size of the slip events and/or their slip velocity, as illustrated in Figure 5. In addition, no dependence of the transition on the values of F_N or F_S is evident. The appearance of a distinct (characteristic) time scale immediately after contact rupture suggests regimes in which qualitatively different physical mechanisms contribute to the interface strength. In the next section we will present a model which may explain these, somewhat unexpected, results.

For each precursory event, slip arrests after ~400μsec and contact renewal process (aging) takes place. This process will not be described here, but is considered in detail elsewhere [17]. We wish to note that *all* of the results described in Figures 3-5 are also observed when for system-sized slip events, with the exception of the ~400μsec finite duration of the dynamics.

4. Discussion

We now consider the implications of the above results. Turning to the detachment phase, we note that the major reduction of contact area happens immediately (within our temporal resolution) and *precedes* the net slip. This leads us to interpret this contact area reduction as the result of rapid (dynamic) fracture. This interpretation is reinforced by the rapid propagation velocities of the detachment fronts. These velocities approach the Rayleigh wave speed, which is limiting velocity of a standard shear crack [18]. Hence, these rapid fronts appear to be variants of the dynamic cracks that typically drive rapid fracture processes. The rapid fluctuation of the displacement just prior to contact detachment is, in this picture, the signature of the approaching crack front that gives rise to the contact reduction. We believe that this rapid fracture process is a distinct process that significantly modifies the

character of the interface. As we will show, the fracture process sets the stage for slip to take place and actively *enables* the ensuing slip dynamics.

The detachment phase is immediately followed by rapid slip at a constant slip velocity which sharply slows down after a characteristic time of ~60μsec. This sharp drop of the slip velocity strongly suggests a sharp increase in the resistance to motion along the interface. This, therefore, corresponds to a dramatic increase in the frictional strength of the material within the interface. As this rapid transition is accompanied by only a small (less than 3%) change in A, we can conclude that, at the transition between the rapid and slow slip regimes, a significant change is taking place in the *other* ingredient of the frictional strength, the shear strength of the contacts, τ. Below, we suggest a fracture-induced weakening mechanism that can account for both the initial weakening of the contacts' shear strength within the detachment phase as well as the subsequent sharp transition to interface strengthening after a constant, (thermally determined) time.

Let us first consider the *tensile* fracture of bulk PMMA. When bulk PMMA undergoes tensile fracture, new surfaces (the fracture surfaces) are created. The fracture energy, Γ, of a bulk material, is defined as the energy cost, per unit area, needed to create these new surfaces. In PMMA, the measured fracture energy is Γ~1500-2000J/m^2. This value is orders of magnitude larger than the energy needed (~1 J/m^2) to fracture a unit area of molecular bonds. Thus, only a small fraction of Γ is actually used to break the molecular "bonds" that bind the surfaces together. The dominant contribution to Γ results from irreversible (plastic) material deformation that occurs prior to bond fracture. This deformation is driven by the enormous stresses that exist in the close vicinity of a crack's tip. These deformation processes involve the internal shear of the long polymer strands within PMMA, which must be stretched to cause their fracture. One result of these large deformations at the tip of a crack is that rapid fracture is accompanied by large and immediate heating of the fracture surface. This occurs because the large amounts of energy generated by plastic deformation are deposited in the very near vicinity (order 1μm) of the fracture surface at a much higher rate than this region can cool via thermal diffusion. As a result

of this process, temperature increases of 500-1000°C have been observed in the tensile fracture of PMMA [19].

We now consider the initiation of *frictional* sliding. The interface is composed of a myriad of interlocking protrusions (or "asperities") that serve as barrier to motion. This picture is schematically shown in the inset of Figure 7. For macroscopic slip to occur, these initially interlocking asperities must continuously and coherently circumvent each other. Can the detachment process be explained by elastic (non-dissipative) deformation of the contacts? This does not seem likely. For elastic contact deformation or dilation [20] to occur, displacements on the order of the protrusion sizes must take place at nearly acoustic time scales. This would necessitate the creation of elastic strains of order unity that are applied at extremely high strain rates. The extreme loading rate is due to the nearly singular stress fields that surround the tips of the crack-like detachment fronts as they propagate across the interface at velocities that approach material sound speeds (Fig. 2).

A more likely scenario would, therefore, be that the contact deformation involves dissipative processes. In general, these processes should involve either fracture, internal damage, or plastic deformation. All of these dissipative processes involve an energy cost proportional to $A(x,t)$. We note that the energy costs involved in all of these processes are not only analogous to the fracture energy of bulk materials, but involve the same types of deformation processes that occur when bulk fracture takes place. Our results indicate that, precisely as in tensile fracture, the dissipative processes participating in interface detachment must take place within very short (~μsec) time scales. In the tensile fracture of PMMA these processes are dominated by extreme plastic deformation. In interface fracture, as in tensile fracture, such processes would result in rapid heating of the thin interface layer where the material deformation occurs.

We can estimate both the magnitude of the temperature increase at the interface and its duration by means of a very simple model. Let us assume that all of the energy involved in the fracture (detachment) process, ΓA, is deposited on the thin (0.1-1μm thick) contact layer of thickness, h, at the

interface. This is justified, since only within this layer do interlocking protrusions circumvent each other in order to enable coherent slip. This energy is deposited "immediately" by the rapidly propagating detachment front. If this process is sufficiently rapid, *all* of this energy will be deposited within the volume Ah. Thus, $\Gamma A = \rho C_P \cdot (Ah) \cdot \Delta T$, where ρ, C_P and ΔT are, respectively, the density (1190kg/m^3), heat capacity (1490 J/(kg·°C)) and temperature rise of PMMA at the interface. This process will then immediately increase the temperature along the layer by $\Delta T \sim \Gamma/(\rho C_P \cdot h)$, where the value of the real contact area, A, plays no role since it factors out of the equation. If we now assume the values of $\Gamma \sim$ 1000-2000 J/m^2 obtained in the tensile fracture of PMMA [21], we find that ΔT approaches the same 500-1000°C values that are observed in bulk fracture.

This large temperature rise drives the frictional interface well beyond the glass temperature, T_g, of PMMA (T_g~110°C). This results in dramatic weakening of the contact shear strength, so that slip is initiated on a highly weakened interface. The surface will not remain in this weakened state over time, however, since the heat deposited within the detachment phase will diffuse away from the interface into the bulk material. Once the interface temperature goes below T_g, its strength will immediately increase.

This cooling time, t_{cool} can be simply estimated. We assume that the heat is initially uniformly deposited between $h/2<z<h/2$. Using a one-dimensional heat diffusion equation [22] to describe the cooling process, one obtains the following expression for the temperature at some distance z_0 from the interface as function of time:

$$T(t) = T_{room} - \frac{\Gamma}{4\rho C_P h}\left[erf\left(\frac{z_0 - h}{\sqrt{4\chi t}}\right) - erf\left(\frac{z_0 + h}{\sqrt{4\chi t}}\right)\right] \qquad (1),$$

where χ=1.1 × 10^{-7}m^2/sec is the thermal diffusivity of PMMA and *erf* the error function.

Let us now assume that t_{cool} corresponds to the experimentally observed duration of the rapid slip phase. Except for the effective value of Γ for interface fracture, all of the parameters in Eq. 1 are now known. The value of Γ for interface (Mode II) fracture may then be estimated by assuming that the time necessary for $T(t)$ to decrease to T_g is the experimentally observed t_{cool}=60μsec. In Figure 6 we present

curves of $T(t)$ obtained for several different values of Γ, for h=1μm and z_0=0.5μm (we chose a value of z_0 that corresponds to the mean thickness of our interface – as schematically shown in the inset of Figure 7). It is evident that t_{cool} depends strongly on Γ (see the inset of Figure 6). We find that the experimental value of t_{cool}=60μsec is obtained for $\Gamma \approx 1400$ J/m^2, which is approximately the magnitude of Γ measured in tensile fracture experiments.

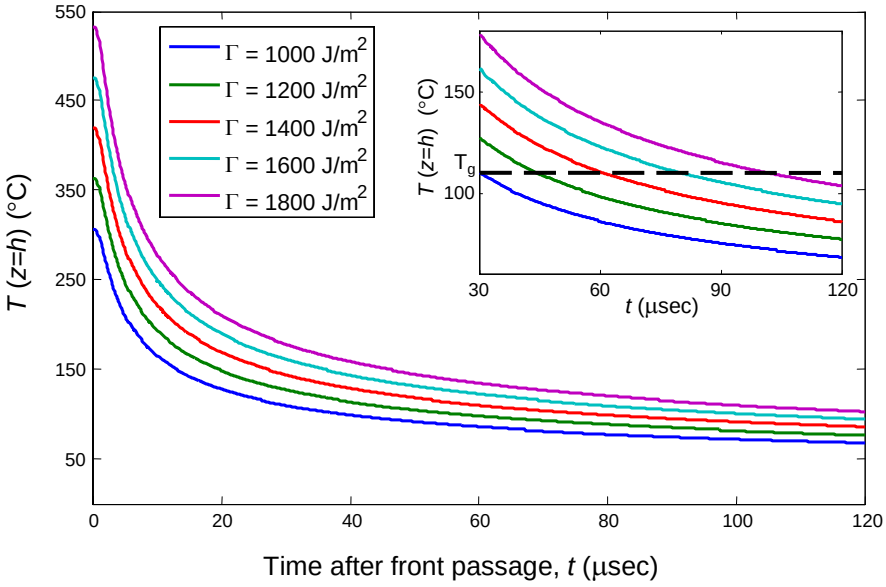

Figure 6. The cooling down process for several values of Γ. The evolution of $T(t)$ at $z=z_0$=0.5μm according to Equation 1 is given, where Γ=1000-1800J/m^2, h=1μm. All curves exhibit a similar qualitative behavior, but the cooling time, t_{cool}, to below T_g is a strong function of Γ. The inset demonstrates that Γ=1400J/m^2 is consistent with the experimentally observed 60μsec transition time.

It is worth noting that the above estimate of t_{cool} is nearly independent of the value of h that we assume. This is demonstrated in Figure 7, where t_{cool} is plotted for values of h ranging from 0.02-2μm, with Γ=1400 J/m^2 and z_0=0.5μm. The near independence of t_{cool} on both h and z_0 results from the fact that the arguments of the *erf* are small. By approximating Eq. 1 to leading order, we find that:

$$t_{cool} = \frac{1}{4\pi\chi}\left[\frac{\Gamma}{\rho C_P\left(T_g - T_{room}\right)}\right]^2 \qquad (2),$$

The above picture is wholly consistent with our experimental results, if we assume that the same dissipative processes that are involved in bulk fracture are at play in interface slip. To understand why

this may be true, we present a qualitative picture for the interlocking asperities comprising the frictional interface. This is described, schematically, in Figure 8. In order for the asperities to circumvent each other they must deform. Contact mechanics [23, 24] tell us that the maximal shear stress within two contacting asperities does *not* occur on the contact surfaces but, instead, well within the asperity interior. Thus, when shear is sufficiently high, plastic deformation initiates and grows at locations that are well within the interiors of the interlocking asperities within the interface. It is this *internal* deformation that ultimately makes the contacts sufficiently malleable to enable slip. Thus, the large value for Γ obtained in Figs. 6 and 7 could be comparable to its value in tensile fracture, since both processes are governed by the same types of plastic deformation over similar (μm) scales.

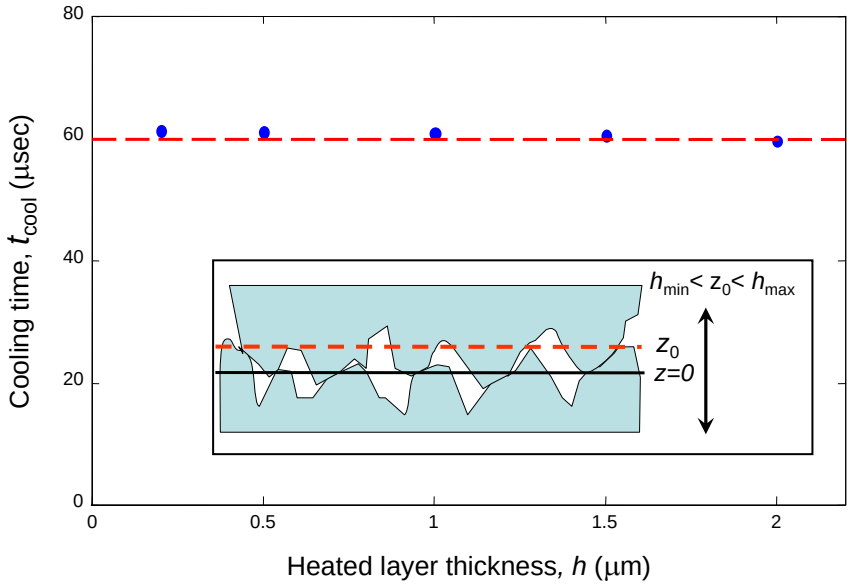

Figure 7. The cooling time, t_{cool}, is nearly independent of the heated layer thickness, h. Plotted is t_{cool} when h is varied from h_{min}=0.2μm to h_{max}=2μm for Γ=1400J/m^2 and z_0=0.5μm. The dashed line depicts the experimentally observed 60μsec transition time. (inset) A schematic drawing of the interface depicting z_0, and range (double arrow) used for h.

Putting all of this together, we have the following qualitative description of the different phases of slip. During the detachment phase (Phase I), plastic deformations occur within the contacts. This causes immediate heating up of the frictional interface beyond the glass temperature of PMMA. This dramatic weakening of the contact shear strength results in the observed rapid slip in Phase II. The subsequent cooling below the glass temperature takes place after a thermally dependent (geometry independent)

characteristic time. When the interface cools to below its glass temperature, its strength sharply increases. This gives rise to the sharp, order of magnitude decrease in slip velocity observed in Phase III.

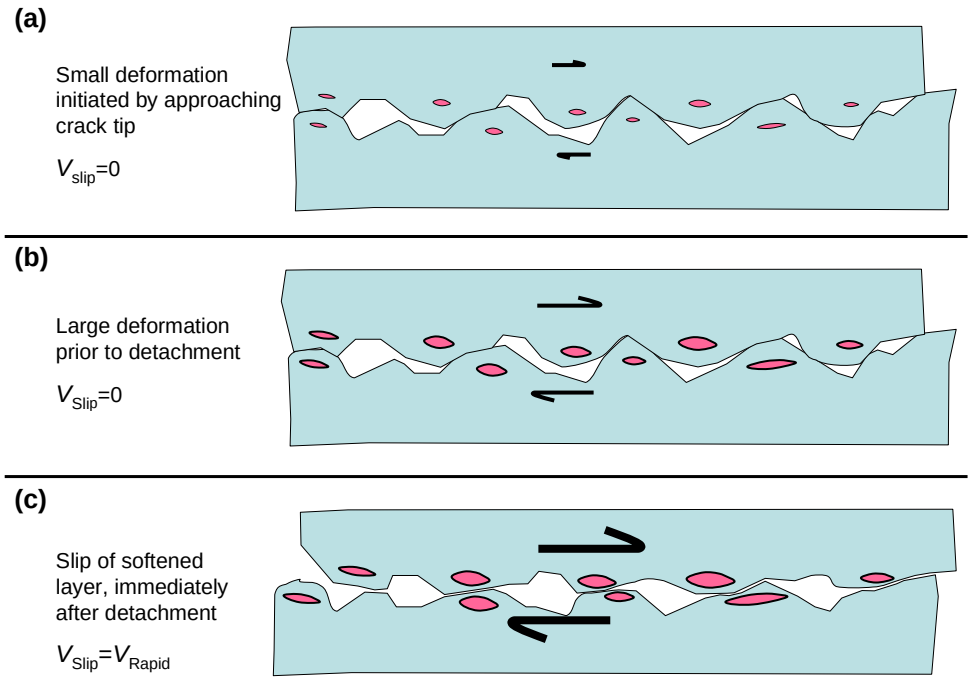

Figure 8. A schematic view of the deformation process within interlocking contacts that results from the rapid (~μsec) passage of a detachment front. **a** Plastic deformation initiates within the contact interiors as the stress field generated by the approaching detachment front starts building up. **b** As the crack tip approaches, the shear stresses at the contacts grow rapidly, causing larger internal deformations and depositing heat within the thin layer surrounding the frictional interface. **c** Finally, the contacts are weakened enough to deform and circumvent each other. This facilitates the rapid slip in Phase II with a velocity V_{Rapid}.

We expect that the local dynamics in Phase III should be analogous to the large-scale frictional motion [25, 26] governed by the contact dynamics of 'rigid' (unsoftened) microcontacts. Whereas the fracture process gives rise to 'collective' heating of the entire ensemble of contacts, in this phase we expect that slip is due to the sporadic rupture of discrete, loosely coupled contacts. Each contact may, itself, heat up when it circumvents its neighbor, but this heating would not be expected to influence the motion of surrounding contacts. Thus, the motion is not influence by collective weakening. In this sense, the interface resembles a glassy system in which the state of each contact is coupled only to that of its neighbors by minute changes of the overall residual shear stress.

The fracture-induced weakening scenario seems qualitatively similar to previously suggested "flash heating" mechanisms [27-29], in which the surface is weakened by the heat generated by very rapid frictional sliding. It is, however, different in two important aspects. First, unlike flash heating, fracture-induced heating takes place *before* any net slip takes place. It is not dependent on whether the resultant slip velocity is rapid or not. The second difference is in the duration of the heat-induced softening. While flash heating will be sustained for as long as the slip is sufficiently rapid, the effects of fracture induced heating last for only as long as it takes the heat deposited on the interface to diffuse away.

Is the suggested scenario general? The mechanism that gives rise to material deformation within interlocked asperities is solely based on rapid shear rates coupled to contact mechanics. This fracture-induced deformation mechanism should, therefore, be a general one. Note that contact deformation *must* occur to enable the otherwise locked asperities to slip. One must now address the question of what deformation mechanism exists for a given material. In acrylics like PMMA, these internal stresses will result in plastic deformation within the interior of the interlocked asperities. In more brittle materials, such as rock, if the asperities do not fracture [30], we speculate that the high stresses within contacts may, instead, lead to internal damage (e.g. substantial internal fracturing or crushing). This will significantly reduce the shear strength of the interlocking asperities, and allow them to easily deform and enable slip. However, unlike acrylics that will re-heal and strengthen upon cooling, the damage in these materials will be retained indefinitely. The re-strengthening of these materials could be a long term process that will only take place long after the slip event is arrested. In these materials, the entire duration of slip will take place on a weakened interface. Evidence of just such internal damage in rock is suggested by recent observations of large "bumps" on the surfaces of active faults. Sagy and Brodsky [31] observed that large fault exposures are populated with large, 10-40 meter, long protrusions. As our model suggests, earthquake-generated slip occurred along the hard exterior surface of these protrusions, whereas their *interior* sections were described as highly deformed. Photographs (taken at the Flowers Pit fault) of both the exterior and interior of objects are presented in Figure 9.

In conclusion, we have presented a rather general scenario of fracture-induced interface weakening that explains the different phases of local slip that are observed in our experiments. We have shown why this scenario might be expected to be of general validity, even when the materials involved in frictional motion can not be described as glassy. The generality of this picture is essentially due to the high loads and loading rate induced by very rapid crack-like fronts that trigger slip. These fronts occur even when the applied loading is quasi-static (as in the experiments described here). When the fronts approach interlocked asperities, the near-singular stresses in the vicinity of their leading edge can only be relieved by stress induced deformation. We have also argued that this scenario is independent of the specific material deformation mechanism. We therefore expect that this picture could play a role in a broad class of sliding systems.

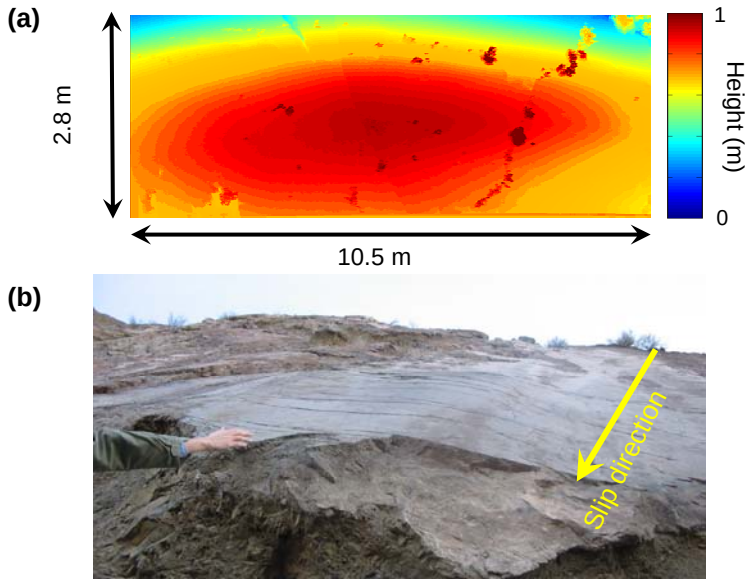

Figure 9. Protrusions on a natural fault (courtesy of A. Sagy). **a** LiDAR height measurements of a geometrical asperity on the Flowers Pit fault. **b** A picture of a different asperity, the cut revealing the highly deformed interior which lies beneath a smooth slip surface.

Acknowledgements: We acknowledge comments A. Sagy, S. M. Rubinstein and G. Cohen. This work, as part of the ESF EUROCORES programme FANAS, was supported by the Israel Science Foundation (grant 57/07). We also acknowledge support of the US–Israel Binational Science Foundation (grant 2006288). J. F. acknowledges the support of the Max Born chair of Natural Philosophy.

References

[1]. Urbakh, M., Klafter, J., Gourdon, D., Israelachvili, J.: The nonlinear nature of friction. Nature 430, 525-528 (2004).

[2]. Scholz, C. H.: Earthquakes and friction laws. Nature 391, 37-42 (1998).
[3]. Dieterich, J. H.: Earthquake Nucleation on Faults with Rate-Dependent and State-Dependent Strength. Tectonophysics 211, 115-134 (1992).
[4]. Marone, C.: Laboratory-derived friction laws and their application to seismic faulting. Annual Review of Earth and Planetary Sciences 26, 643-696 (1998).
[5]. Ben-Zion, Y.: Collective Behavior of Earthquakes and Faults: Continuum-Discrete Transitions, Progressive Evolutionary Changes, and Different Dynamic Regimes. Reviews of Geophysics 46, (2008).
[6]. Bowden, F. P., Tabor, D.: The Friction and Lubrication of Solids. Oxford Univ. Press, New York, pp Pages (2001).
[7]. Ben-Zion, Y.: Dynamic ruptures in recent models of earthquake faults. J. Mech. Phys. Solids 49, 2209-2244 (2001).
[8]. Xia, K., Rosakis, A. J., Kanamori, H.: Laboratory Earthquakes: The Sub-Rayleigh-to-Supershear Rupture Transition. Science 303, 1859-1861 (2004).
[9]. Rubinstein, S. M., Cohen, G., Fineberg, J.: Detachment fronts and the onset of dynamic friction. Nature 430, 1005-1009 (2004).
[10]. Rubinstein, S. M., Cohen, G., Fineberg, J.: Dynamics of precursors to frictional sliding. Phys. Rev. Lett. 98, 226103 (2007).
[11]. Landau, L. D., Lifshitz , E. M.: Theory of Elasticity. Course of Theoretical Physics 7, 96 (1959).
[12]. Rubinstein, S. M., Shay, M., Cohen, G., Fineberg, J.: Crack like processes governing the onset of frictional slip. Int. J. of Fracture 140, 201-212 (2006).
[13]. Greenwood, J. A., Williams, J. B. P.: Contact of nominally flat surfaces. Proceedings of the Royal Society of London, Series A (Mathematical and Physical Sciences) 295, 300-319 (1966).
[14]. Dieterich, J. H., Kilgore, B. D.: Direct Observation of Frictional Contacts - New Insights for State-Dependent Properties. Pure Appl. Geophys. 143, 283-302 (1994).
[15]. Rubinstein, S., Cohen, G., Fineberg, J.: Contact Area Measurements Reveal Loading-History Dependence of Static Friction. Phys. Rev. Lett. 96, (2006).
[16]. Rubinstein, S. M., Cohen, G., Fineberg, J., Reches, Z., in Meso-Scale Shear Physics in Earthquake and Landslide Mechanics Y. H. Hatzor, J. Sulem, V. I., Eds. (CRC Press, 2010) pp. 17-24.
[17]. Ben-David, O., Rubinstein, S. M., Fineberg, J.: Slip-stick and the evolution of frictional strength. Nature 463, 76-79 (2010).
[18]. Freund, L. B.: Dynamic Fracture Mechanics. Cambridge, New York, pp Pages (1990).
[19]. Fuller, K. N. G., Fox, P. G., Field, J. E.: Temperature Rise at Tip of Fast-Moving Cracks in Glassy Polymers. Proceedings of the Royal Society of London Series A-Mathematical Physical and Engineering Sciences 341, 537-557 (1975).
[20]. Marone, C., Raleigh, C. B., Scholz, C. H.: Frictional Behavior and Constitutive Modeling of Simulated Fault Gouge. J. Geophys. Res.-Solid Earth 95, 7007-7025 (1990).
[21]. Sharon, E., Fineberg, J.: Confirming the continuum theory of dynamic brittle fracture for fast cracks. Nature 397, 333-335 (1999).
[22]. L.D., L., Lifshitz , E. M.: Fluid Mechanics. pp Pages (1959).
[23]. Johnson, K. L.: Contact mechanics and the wear of metals. Wear 190, 162-170 (1995).
[24]. Brizmer, V., Kligerman, Y., Etsion, I.: Elastic-plastic spherical contact under combined normal and tangential loading in full stick. Tribol. Lett. 25, 61-70 (2007).
[25]. Dieterich, J. H.: Modeling of Rock Friction .1. Experimental Results and Constitutive Equations. J. Geophys. Res.-Solid Earth 84, 2161-2168 (1979).
[26]. Rice, J. R., Ruina, A. L.: Stability of Steady Frictional Slipping. Journal of Applied Mechanics 50, 343-349 (1983).
[27]. Rice, J. R.: Heating and weakening of faults during earthquake slip. J. Geophys. Res.-Solid Earth 111, (2006).

[28]. Nielsen, S., Di Toro, G., Hirose, T., Shimamoto, T.: Frictional melt and seismic slip. J. Geophys. Res.-Solid Earth 113, (2008).
[29]. Beeler, N. M., Tullis, T. E., Goldsby, D. L.: Constitutive relationships and physical basis of fault strength due to flash heating. J. Geophys. Res.-Solid Earth 113, (2008).
[30]. Wang, W. B., Scholz, C. H.: Wear Processes During Frictional Sliding of Rock - a Theoretical and Experimental-Study. J. Geophys. Res.-Solid Earth 99, 6789-6799 (1994).
[31]. Sagy, A., Brodsky, E. E.: Geometric and rheological asperities in an exposed fault zone. J. Geophys. Res.-Solid Earth 114, B02301 (2009).